

GPU Acceleration of SQL Analytics on Compressed Data

Ze Zhou Huang*, Krystian Sakowski, Hans Lehnert, Wei Cui, Carlo Curino, Matteo Interlandi,
Marius Dumitru, Rathijit Sen

Microsoft

{zacharyhuang, krsakows, weicu, mariusd, firstname.lastname}@microsoft.com

ABSTRACT

GPUs are uniquely suited to accelerate (SQL) analytics workloads thanks to their massive compute parallelism and High Bandwidth Memory (HBM)—when datasets fit in the GPU HBM, performance is unparalleled. Unfortunately, GPU HBMs remain typically small when compared with lower-bandwidth CPU main memory. Besides brute-force scaling across many GPUs, current solutions to accelerate queries on large datasets include leveraging data partitioning and loading smaller data batches in GPU HBM, and hybrid execution with a connected device (e.g., CPUs). Unfortunately, these approaches are exposed to the limitations of lower main memory and host-to-device interconnect bandwidths, introduce additional I/O overheads, or incur higher costs. This is a substantial problem when trying to scale adoption of GPUs on larger datasets. Data compression can alleviate this bottleneck, but to avoid paying for costly decompression/decoding, an ideal solution must include computation primitives to operate directly on data in compressed form.

This is the focus of our paper: a set of new methods for running queries directly on light-weight compressed data using schemes such as Run-Length Encoding (RLE), index encoding, bit-width reductions, and dictionary encoding. Our novelty includes operating on multiple RLE columns without decompression, handling heterogeneous column encodings, and leveraging PyTorch tensor operations for portability across devices. Experimental evaluations show speedups of an order of magnitude compared to state-of-the-art commercial CPU-only analytics systems, for real-world queries on a production dataset that would not fit into GPU memory uncompressed. This work paves the road for GPU adoption in a much broader set of use cases, and it is complementary to most other scale-out or fallback mechanisms.

1 INTRODUCTION

The massive compute parallelism and multi-TB/sec device memory bandwidths of modern GPUs make them attractive for accelerating SQL analytics queries [35, 39]. However, one challenge is that the high-bandwidth memory (HBM) capacity on GPUs is much less, usually by integer factors or an order of magnitude, compared to lower-bandwidth main memory capacity in modern high-end CPU servers. This restricts the dataset sizes that can be processed on GPUs without requiring data movement at run time over slow CPU-GPU interconnects¹, or doing CPU-GPU hybrid processing [36], or using multiple GPUs [13, 28, 29, 37, 46] which increases costs.

*Work done during an internship at the Microsoft Gray Systems Lab while affiliated with Columbia University.

¹ PCIe4 has a bandwidth of 31.5 GB/sec; 63 GB/sec for PCIe5. However, NVLink-C2C can achieve up to 450 GB/sec. This is in contrast to GPU’s HBM bandwidths: e.g., A100s have a memory bandwidth of 2TB/sec, 3.35 TB/sec for H100s, and 5.3 TB/sec for MI300Xs. In comparison, a typical CPU server can have up to 0.5 TB/sec.

One approach to alleviate this bottleneck is to run queries on compressed data, which is the focus of this paper. We focus on light-weight encodings for compression, in particular, run-length encoding (RLE) for consecutively repeating values, index encoding for sparse data, dictionary encoding, and bit-width reductions. Our methods not only allow GPU query processing on datasets that would not fit uncompressed in the GPU HBM, but also achieve high performance by leveraging redundancy eliminated by compression.

Being able to operate directly on RLE data provides both space and time advantages. The representation uses constant space, *regardless of the length of the run*. In contrast, an uncompressed representation uses space that is directly proportional to the number of values, that is, the length of the run. This reduces GPU HBM capacity requirements. Operating on RLE data can also be faster. For example, a SUM operation over an RLE data column would need to multiply the run values with the run lengths, then add the results over all runs, whereas in a plain/uncompressed representation, every value in the column needs to be scanned. Additionally, the space savings with RLE reduces I/O overheads for data movement between the GPUs and other devices, e.g., CPU-GPU data transfers over the (relatively) low-bandwidth PCIe bus.

SQL query processing directly on RLE data, however, is challenging when operations involve multiple data columns. This is because of misalignment in runs between columns that can occur due to different data distributions as well as effect of predicate filters on different columns. Continuing with the above example, SUM (A+B) on two RLE columns A and B is not straightforward to implement since runs in A and B can start and end at different positions, making a direct step of adding the run values between the two columns impossible. While this can be handled with an iterative approach that loops through the different runs and keeps track of their start and end positions, such an approach is inefficient on parallel computational backends such as GPUs due to severe under-utilization of resources. Additional complexities arise with heterogeneous encoding schemes across columns, e.g., if A uses RLE, but B uses an index representation that is more suitable for non-repetitive sparse data.

While prior works [6, 27, 40] have recognized and exploited the space-savings advantages of RLE data, they usually decompress the data in the GPU memory hierarchy, shared memory, and registers before using them as inputs to relational operator implementations. Some works study the potential for query processing over partially compressed data, but focus mostly on specific operations such as table scan [15] or join [49] without providing a comprehensive framework for all relational operators. In contrast, we develop *novel parallel algorithms and a framework for SQL relational operators to: (1) directly operate on encoded data as much as possible without decompressing them, and (2) be efficiently implemented on parallel devices such as GPUs*. Our methods provide query run time

speedups of an order of magnitude compared to state-of-the-art CPU-only relational engines for representative production queries on a production dataset that is larger than the HBM capacity of a single A100 GPU in uncompressed form. To make our implementations easily portable to multiple accelerators, we use the same approach as TQP [17, 18] and implement SQL queries using PyTorch tensor programs, but extend it to show how PyTorch functions can be used to implement relational operators for compressed data.

In summary, we extend the state of the art in the following ways.

- We show how SQL operations can be performed on data encoded for compression, particularly RLE data, in GPUs *without expanding as much as possible*, in contrast to traditional approaches.
- We demonstrate for the first time how this can be done in TQP with PyTorch tensor operations.
- We show query run time speedups of an order of magnitude compared to state-of-the-art CPU-only database and analytical systems on a real-world dataset that is too large to fit into the HBM of a high-end GPU without compression.

As far as we know this is the first work showcasing a comprehensive framework allowing to execute complex queries (e.g., including joins, group by, aggregation, projection and filter operators) end to end on lightweight-compressed data in GPU.

The rest of the paper is organized as follows. Section 2 briefly describes the tensor approach used by TQP that we leverage in this work. Section 3 presents the encoding schemes for compression that we use. Section 4 introduces our novel and parallel implementations of core transformations on compressed data. Sections 5–8 show how we use them in novel ways to efficiently implement relational operators on GPUs. Section 9 presents experimental results and speedups with our techniques. Section 10 discusses related work and Section 11 concludes the paper.

2 BACKGROUND: TQP

The Tensor Query Processor (TQP) [7, 18] converts SQL queries into tensor programs, then runs them using Tensor Computation Runtimes (TCRs), such as PyTorch, on hardware backends such as GPUs [9, 17, 18] and APUs [11]. This makes TQP easily portable to different devices while at the same time benefiting from the optimizations provided by the TCRs. In this work, we continue to use TQP’s approach to get the same portability and performance advantages, but extend it to show how we can convert queries to tensor programs that can operate on lightweight-compressed data.

TQP supports input tabular data from files in Parquet [16] and CSV formats, and from in-memory formats such as NumPy [44] and Pandas DataFrames [30]. TQP converts each input column into PyTorch tensors. The conversion is straightforward for numeric and date columns. TQP does not currently support decimals, and instead represents them using floating-point numbers. ASCII string columns are value-encoded and dictionary-encoded. At the end of the conversion process, every column is represented using one or more numeric PyTorch tensors. The conversion step is done offline, before running queries.

Given an input SQL query, TQP uses a query optimizer (currently, Apache Spark’s [50] Catalyst optimizer) to obtain a physical query plan. It then converts it into an equivalent tensor program [18]. It loads tensors corresponding to the input columns needed by the

query into the device memories—for GPUs, this is the High Bandwidth Memory (HBM) which is available as global memory on the GPUs. TQP loads and operates on entire columns, spanning all rows of the table, rather than splitting them up into smaller chunks. This is beneficial for good performance as it avoids overheads of repeated sets of kernel launches and improves GPU resource utilization, but requires the full column tensor (in addition to temporary results) to fit in the available HBM capacity. In this work, we continue with TQP’s approach of loading and operating on full columns, but additionally allow compact representation for encoded data, thereby reducing the memory requirements, as we discuss next.

3 ENCODINGS FOR COMPRESSION AND THEIR TENSOR REPRESENTATIONS

In order to enable query processing on compressed data, we expand the encodings supported in TQP. We add support for two additional light-weight encoding techniques—Run-Length Encoding (RLE) and indexing. RLE is useful for compactly representing sequences of consecutively repeating values. We use indexing in novel ways, including to separate outliers and enable compression through bit-width reduction, and for efficient representation of sparse data. Currently we do not support operations on data in heavy-weight compression formats, e.g., Snappy, zstd, LZ4, gzip, etc.

3.1 Basic Encodings

First, we list the types of basic encodings for columns that we support and their tensor representations. These are applied on top of any dictionary encodings of values, e.g., for string columns.

- **Plain:** This is the existing tensor representation used by TQP as we discussed in Section 2. For every column, there is a 1:1 mapping from a row position in the column to the corresponding position in the tensor representing the values in the column.
- **RLE:** We use three tensors to represent a set of RLE runs: (1) values (v), (2) start positions (s), and (3) end positions (e). Tensors v , s , and e are of equal length, and the i^{th} entry represents a run with value v_i spanning row numbers in the closed and continuous interval $[s_i, e_i]$. The positions are zero-based and unique. Tensors v , s , e are sorted by s (equivalently, by e). Note that, we could have used a tensor for run lengths (l) instead of for end positions (e). We can choose either lengths or end positions based on convenience, and calculate the other at run time using the equation: $l = e - s + 1$. Runs are non-overlapping by position.
- **Index:** We use two tensors to represent index encoding: (1) values (v), and (2) positions (p). Tensors v and p are of equal length, sorted by p , and the i^{th} entry represents value v_i at row number p_i . The positions are zero-based and unique.

While Plain encoding has an implicit 1:1 correspondence between row numbers and positions in the tensor representation, RLE and Index encoding explicitly track row numbers. This also allows for efficient representation when there are gaps in the underlying data, e.g., when some portions of the column are de-selected after application of filter predicates. Thus, for RLE, for two consecutive entries at tensor positions i and $i + 1$, we have $s_{i+1} \geq e_i + 1$. Similarly, for Index encoding, we have $p_{i+1} \geq p_i + 1$. In contrast, Plain encoding does not allow for gaps in the tensor representation.

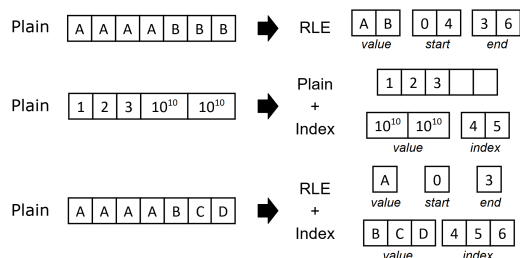


Figure 1: GPU-Optimized Tensor Data Representations.

3.2 Composite Encodings

In addition to basic encodings, we also introduce the following novel composite encodings that combine Index with Plain and RLE to enable further compression.

- **Plain + Index:** PyTorch requires a uniform data type for all elements within a single tensor. However, outliers can force the entire tensor to use a larger data type than necessary. To enable bit-width reduction with narrower data types, we can combine Plain with Index encoding. We store most values in one PyTorch tensor with a narrower type and represent the outliers separately using Index encoding.
- **RLE + Index:** RLE works best for continuous value segments. However, some columns may contain both continuous (pure) and non-continuous (impure) segments. While impure segments can be represented by a series of unit-length RLE runs, this can be inefficient since each run is represented by three elements (value, start, end). Instead, we can handle impure segments with Index encoding. The Index positions and the RLE intervals are disjoint in this composite encoding.

Note that our bit-width reduction differs from traditional CPU compression techniques. While CPU approaches break columns into small groups to optimize bit width and combine with techniques like DELTA and FOR [3, 4, 51], the small groups suit poorly for GPU processing. Instead, we leverage PyTorch’s preference for large tensors by using index-based outlier separation. After removing outliers, we apply centering to reduce bit width. Centering is similar to FOR, but instead of local reference values (typically minimum in each group) we use a global reference value of the mid-range for the entire column. This allows us to represent most values with narrower bit widths while handling outliers separately, achieving good compression without sacrificing GPU execution efficiency.

EXAMPLE 1. Consider the various optimized Tensor representations for Data Compression in Figure 1.

Plain → RLE example: The sequence $[A, A, A, A, B, B, B]$ is compressed using run-length encoding. A repeats from positions 0 to 3, and B repeats from positions 4 to 6. We store this as $v = [A, B], s = [0, 4], e = [3, 6]$. This captures exactly where each value run begins and ends.

Plain → Plain + Index example: When handling a column with values $[1, 2, 3, 10^{10}, 10^{10}]$, the outliers at indices 4 and 5 would force the entire tensor to use a larger data type. We separate the data: regular values in Plain tensor $[1, 2, 3]$ and outliers in a separate value tensor $[10^{10}, 10^{10}]$ with their positions in index tensor $[4, 5]$. In a dataset with 1 billion elements, if a few outliers require int64 but most values fit in int8, Plain representation would force all

values into int64, using 8 GiB of memory (8 bytes \times 1 billion). With Plain + Index, we store most values in int8 (1 GiB) plus a small overhead for outliers and their indices, saving ~ 7 GiB of memory while preserving all data values.

Plain → RLE + Index example: The sequence $[A, A, A, A, B, C, D]$ has a consecutive run of A (positions 0-3) but B and C do not form runs. We use RLE for the A run ($v = [A], s = [0], e = [3]$) and Index encoding for the scattered values ($v = [B, C, D], p = [4, 5, 6]$).

3.3 Data and Mask column representations

Our encoding schemes are versatile and can be used to represent: (1) data columns containing actual values from database tables and intermediate results, (2) mask columns that encode boolean predicates for selections and filters, and (3) internal data structures required by query operators. This unified representation approach allows our system to maintain a consistent execution model while adapting to different data characteristics and query requirements.

While encoding approaches for data and mask columns are similar, there are a few differences in their representations as follows.

- The domain of values for masks is restricted to $\{T, F\}$.
- Since there are no outliers in values, the composite Plain + Index encoding is not applicable for masks.
- In position-explicit encodings (RLE, Index) for masks, only positions corresponding to T values are maintained in the tensor representations. Plain encoding tracks both T and F values.
- In position-explicit encodings (RLE, Index) for masks, the value tensor (v) is not needed, since all tracked values are implicitly equal to T .

Depending on the operator type, the operands can be data columns, mask columns, scalar expressions, or literals. Result columns can be data or masks. We will use the terms DataColumn and MaskColumn where needed to distinguish between these two types.

4 PRIMITIVES

We develop a set of novel parallel algorithms to implement fundamental operations on encoded data types. These operations include conversion between encodings, detecting containment and overlap between position-explicit encodings, positional range intersection and union, compaction, etc. Table 1 lists the set of non-trivial operations. These operations can be used as building blocks to implement more complex operations. In Sections 5–8 we describe how we implement relational operators using these fundamental operations.

Due to space limitation, in this section we include pseudo-code only for a few primitives, notably the intersection primitives that are heavily used for implementing relational operators. Functions in **bold font** are provided by PyTorch and have been optimized by PyTorch developers for different backends including GPUs. Note that there are no explicit for loops or conditional checks in the codes, which helps to maximize utilization of the available hardware parallelism.

4.1 Range Intersection

This operation finds the intersection of two sorted lists of ranges. We use this operation frequently in computations involving multiple RLE columns. At the end of the intersect, all columns will have the

Table 1: Fundamental Operations for Encoded data.

| Primitive | Description |
|----------------------|---|
| range_intersect | Intersection of RLE runs |
| idx_in_rle | Intersection of Index and RLE data |
| idx_in_idx | Intersection of Index columns |
| rle_contain_idx | Index positions contained within an RLE run |
| range_union | Union of RLE runs |
| merge_sorted_idx | Merge sorted Index tensors |
| compact_rle | Remove gaps between runs of RLE data |
| compact_rle+index | Remove gaps in RLE + Index data |
| complement_rle | Complement of RLE intervals |
| complement_index | Complement of Index positions |
| rle_to_index | Convert RLE data to Index |
| rle_to_plain | Convert RLE data to Plain |
| plain_to_rle | Convert Plain data to RLE |
| plain_to_rle+index | Convert Plain data to Composite (RLE+Index) |
| plain_to_plain+index | Convert Plain data to Composite (Plain+Index) |

same number of runs and same start and end positions (same s and e tensors for all columns) corresponding to position ranges that are common to all input columns. If a range is split, the value is duplicated for the new ranges. Our goal is to minimize the number of range splits (i.e., maximize run lengths) in the result.

Our approach is inspired by bioinformatics techniques for chromosome range intersections [25], as detailed in Algorithm 1. The "range_intersect" algorithm efficiently computes the intersection of two RLE inputs, c_1 and c_2 , by first bucketizing the start ($c_1.s$) and end ($c_1.e$) points of the first input relative to the second (Lines 1-2). It then counts intersections (Line 3) and generates index tensors idx_1 and idx_2 for each intersecting range (Lines 4-6), using the helper function range_arange (Algorithm 2) for idx_2 . Unlike PyTorch's `arange`, which operates on single start/length values, range_arange accepts tensors of starts and lengths to generate multiple concatenated sequences. Finally, the algorithm determines the start and end points of the intersections (Lines 7), producing the resulting tensors s and e . To optimize performance, the input with the fewer ranges should always be used as c_1 .

Algorithm 1 range_intersect

Input: RLE columns c_1, c_2
Output: Intersection start and end positions s, e

```

1:  $bin_s \leftarrow \text{bucketize}(c_1.s, c_2.e, \text{right}=\text{False})$ 
2:  $bin_e \leftarrow \text{bucketize}(c_1.e, c_2.s, \text{right}=\text{True})$ 
3:  $cnt \leftarrow bin_e - bin_s$ 
4:  $arange \leftarrow \text{arange}(\text{len}(cnt))$ 
5:  $idx_1 \leftarrow \text{repeat\_interleave}(arange, cnt)$ 
6:  $idx_2 \leftarrow \text{range\_arange}(bin_s, cnt)$ 
7:  $s, e \leftarrow \text{max}(c_1.s[idx_1], c_2.s[idx_2]), \text{min}(c_1.e[idx_1], c_2.e[idx_2])$ 
8: return  $s, e$ 

```

EXAMPLE 2. Consider the range intersection between the positional ranges of two RLE masks, c_1 and c_2 , as shown in Figure 2. Mask c_1 has a single range represented as $c_1.s = [2], c_1.e = [7]$. Mask c_2 has three ranges represented as $c_2.s = [1, 4, 6], c_2.e = [3, 5, 8]$. Recall that masks only represent ranges corresponding to a value of T .

To compute their intersection using the range_intersect algorithm (Algorithm 1):

- **Step 1: Bucketize start positions.** We bucketize the start position ($c_1.s$) of Mask c_1 relative to the end positions ($c_2.e$) of Mask

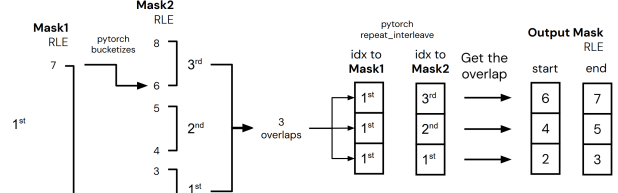
Algorithm 2 range_arange (helper function)

Input: $start, length$
Output: Concatenated sequence $result$

```

1:  $t \leftarrow \text{cumsum}(length)$ 
2:  $t \leftarrow \text{cat}([0, t[:-1]])$  // prepends 0, includes all but last element
3:  $total\_size \leftarrow \text{sum}(length)$ 
4:  $result \leftarrow \text{repeat\_interleave}(start, length)$ 
5:    $+\text{arange}(total\_length)$ 
6:    $-\text{repeat\_interleave}(t, length)$ 
7: return  $result$ 

```


Step 1: get # overlaps for ranges in parallel

Step 2: get start/end for overlaps in parallel

Figure 2: Illustration of range_intersect algorithm for AND between RLE masks: bucketization identifies overlaps, then parallel PyTorch operations compute precise intersections.

$c_2.bin_s = \text{bucketize}([2], [3, 5, 8]) = [0]$. This means the start point 2 comes before the first end point 3.

- **Step 2: Bucketize end positions.** We bucketize the end positions ($c_1.e$) of Mask c_1 relative to the start positions ($c_2.s$) of Mask c_2 . $bin_e = \text{bucketize}([7], [1, 4, 6], \text{right} = \text{True}) = [3]$. This means the end point 7 comes after all start positions in c_2 .
- **Step 3: Count overlaps.** We count the overlaps by subtracting bin_s from bin_e . $cnt = bin_e - bin_s = [3] - [0] = [3]$. This indicates that the range in c_1 overlaps with all 3 ranges in c_2 .
- **Step 4: Create index tensors.** We create index tensors that identify which ranges from each mask participate in each overlap. $idx_1 = \text{repeat_interleave}([0], [3]) = [0, 0, 0]$ (indices into c_1) and $idx_2 = \text{range_arange}([0], [3]) = [0, 1, 2]$ (indices into c_2).
- **Step 5: Compute intersection points.** We compute the actual intersection points by taking the maximum of start points and minimum of end points. $s = \text{max}(c_1.s[idx_1], c_2.s[idx_2]) = \text{max}([2, 2, 2], [1, 4, 6]) = [2, 4, 6]$ and $e = \text{min}(c_1.e[idx_1], c_2.e[idx_2]) = \text{min}([7, 7, 7], [3, 5, 8]) = [3, 5, 7]$.

So, the final output is an RLE mask with $s = [2, 4, 6]$ and $e = [3, 5, 7]$, representing exactly the segments where both input masks c_1 and c_2 have True values.

4.2 Index Intersection

These operations handles intersections for Index encoded data ($c.p$). A common task is finding which positions ($c_{idx.p}$) from an Index list fall within any RLE ranges ($c_{rle.s}, c_{rle.e}$). We provide two algorithms for this: `idx_in_rle` (Algorithm 3) and `rle_contain_idx` (Algorithm 5). The main computational work involves the bucketize operation performed by each. `idx_in_rle` uses `bucketize(c_{idx.p}, c_{rle.s})`, while `rle_contain_idx` uses `bucketize(c_{rle.s}, c_{idx.p})` and `bucketize(c_{rle.e}, c_{idx.p})`. The choice between them for optimal performance depends on the relative input sizes: `idx_in_rle` is

generally preferred when $|c_{idx.p}| \ll |c_{rle.s}|$. We also provide `idx_in_idx` (Algorithm 4) for intersecting two Index lists.

EXAMPLE 3 (`idx_in_rle`). *Let us consider `idx_in_rle` with an Index column c_{idx} and an RLE column c_{rle} . Suppose $c_{idx.p} = [2, 4, 7]$ and $c_{rle.s} = [0, 6]$, $c_{rle.e} = [2, 7]$. We want to find which elements in $c_{idx.p}$ fall within the RLE ranges $[0-2]$ or $[6-7]$ defined by c_{rle} .*

- **Step 1: Bucketize positions.** `bucketize($c_{idx.p}, c_{rle.s}, right=True$)` gives $[1, 1, 2]$. Subtracting 1 yields $bin = [0, 0, 1]$. This tells us which RLE range each position p might belong to (position 2 maps to range 0, 4 maps to range 0, 7 maps to range 1).
- **Step 2: Verify containment.** We check two conditions for each position p in $c_{idx.p}$: (1) $bin \geq 0$ ensures the position isn't before the first start s in $c_{rle.s}$, and (2) $p \leq c_{rle.e}[bin]$ ensures the position is not past the end e of its assigned RLE range. For position 2: $bin=0$. $0 \geq 0$ (T) and $2 \leq c_{rle.e}[0] = 2$ (T). 2 is included. For position 4: $bin=0$. $0 \geq 0$ (T) and $4 \leq c_{rle.e}[0] = 2$ (F). 4 is excluded. For position 7: $bin=1$. $1 \geq 0$ (T) and $7 \leq c_{rle.e}[1] = 7$ (T). 7 is included.
- **Step 3: Apply mask.** The resulting mask is $[T, F, T]$. Applying this to $c_{idx.p}$ gives the final result $p_{out} = [2, 7]$.

Algorithm 3 `idx_in_rle`

Input: Index column c_{idx} , RLE c_{rle}
Output: Result positions p_{out}

- 1: $bin \leftarrow \text{bucketize}(c_{idx.p}, c_{rle.s}, right=True)$
- 2: $bin \leftarrow bin - 1$
- 3: $mask \leftarrow (bin \geq 0) \wedge (c_{idx.p} \leq c_{rle.e}[bin])$
- 4: **return** $c_{idx.p}[mask]$

Algorithm 4 `idx_in_idx`

Input: Index columns c_1, c_2
Output: Result positions

- 1: $bin \leftarrow \text{bucketize}(c_1.p, c_2.p, right=True) - 1$
- 2: $mask \leftarrow (bin \geq 0) \wedge (c_1.p = c_2.p[bin])$
- 3: **return** $c_1.p[mask]$

EXAMPLE 4 (`rle_contain_idx`). *Let us illustrate `rle_contain_idx` using the same input data as the `idx_in_rle` example for direct comparison. Suppose $c_{idx.p} = [2, 4, 7]$ and the RLE column c_{rle} has ranges defined by $c_{rle.s} = [0, 6]$ and $c_{rle.e} = [2, 7]$. The ranges are $[0-2]$ and $[6-7]$. We want to find which positions in $c_{idx.p}$ are contained within any of these RLE ranges.*

- **Step 1: Bucketize RLE starts.** We bucketize each RLE start position ($c_{rle.s}$) against the sorted index positions ($c_{idx.p}$). $bin_s = \text{bucketize}(c_{rle.s}, c_{idx.p}) = \text{bucketize}([0, 6], [2, 4, 7]) = [0, 2]$. (0 is before index 0 value '2'; 6 is before index 2 value '7').
- **Step 2: Bucketize RLE ends.** We bucketize each RLE end position ($c_{rle.e}$) against $c_{idx.p}$, using `right = True` and subtracting 1. $bin_e = \text{bucketize}(c_{rle.e}, c_{idx.p}, right=True) - 1 = \text{bucketize}([2, 7], [2, 4, 7], right=True) - 1 = [1, 3] - 1 = [0, 2]$. (2 is \leq index 0 value 2, giving index 1; 7 is \leq index 2 value 7, giving index 3. Then subtract 1).
- **Step 3: Create mask.** We create a mask where $bin_s \leq bin_e$. $mask = (bin_s \leq bin_e) = ([0, 2] \leq [0, 2]) = [True, True]$.
- **Step 4: Apply mask.** We apply $mask$ to bin_s and bin_e . They remain unchanged: $bin_s = [0, 2]$, $bin_e = [0, 2]$.
- **Step 5: Convert RLE indices to position indices.** We use `rle_to_index` to generate the flat list of indices into $c_{idx.p}$ that correspond to the ranges defined by the masked bin_s and bin_e .

For range 1 ($s = 0, e = 0$): indices $[0]$. For range 2 ($s = 2, e = 2$): indices $[2]$. Combined indices: $[0, 2]$. Let this result be idx_{flat} .

- **Step 6: Gather positions.** We select the positions from $c_{idx.p}$ using `idx_flat`: $p_{out} = c_{idx.p}[idx_{flat}] = c_{idx.p}[[0, 2]] = [2, 7]$.

The final output is $p_{out} = [2, 7]$, which are exactly the positions from $c_{idx.p}$ that fall within the RLE ranges $[0-2]$ or $[6-7]$. This matches the output of the `idx_in_rle` example for the same input.

Finally, the `idx_in_idx` algorithm (Algorithm 4) works similarly to `idx_in_rle`, using `bucketize` to find potential matches between two sorted position lists ($c_1.p, c_2.p$) and then verifying exact equality.

Algorithm 5 `rle_contain_idx`

Input: Index column c_{idx} , RLE column c_{rle}

Output: Result positions p_{out}

- 1: $bin_s \leftarrow \text{bucketize}(c_{rle.s}, c_{idx.p})$
- 2: $bin_e \leftarrow \text{bucketize}(c_{rle.e}, c_{idx.p}, right=True) - 1$
- 3: $mask \leftarrow (bin_s \leq bin_e)$
- 4: $bin_s, bin_e \leftarrow bin_s[mask], bin_e[mask]$
- 5: **return** $c_{idx.p}[\text{rle_to_index}(bin_s, bin_e)]$

5 LOGICAL OPERATIONS

Logical operators (AND, OR, NOT) operate on `MaskColumns` as input operands and produce a `MaskColumn` as result.

5.1 AND

We summarize the design of this operator in Table 2.

- **Plain mask AND Plain mask:** This is a straightforward boolean operation using PyTorch's logical AND operator (`&`). For example, if we have two Plain masks $[T, F, T, F]$ and $[T, T, F, F]$, the result would be $[T, F, F, F]$.
- **RLE mask AND RLE mask:** We implement this using the `range_intersect` operation (Algorithm 1).
- **RLE mask AND Plain mask:** Directly performing AND between an RLE mask and a Plain mask is inefficient because it requires searching for each 'True' value in the Plain mask. A more efficient approach is to convert the RLE mask into either an Index mask (`rle_to_index`) or a Plain mask (`rle_to_plain`), and then apply the AND operation following Table 2. The choice depends on the sparsity of the RLE mask: if sparse, convert to an Index mask; otherwise, convert to a Plain mask.
- **RLE mask AND Index mask:** This operation checks whether each index value in the Index mask falls within any range specified by the RLE mask. PyTorch's `bucketize` function provides native support for this step. Depending on the relative sizes of the masks, we either use the Index mask to bucketize the RLE mask (`idx_in_rle`) or use the RLE mask to bucketize the Index mask (`rle_contain_idx`).
- **Plain mask AND Index mask:** This operation selects index values where the corresponding positions in the Plain tensor are 'True', using PyTorch's subscript operator (`[]`).
- **Index mask AND Index mask:** This operation checks whether each value in one index tensor also appears in the other one. This can be efficiently performed using bucketization, with the larger tensor chosen as the bucketized input.

Table 2: Implementation Design of Physical Operator for AND between *Columns* (§ 5.1), Alignment (§ 6) and Apply Join Index (§ 8.2). **Unsorted RLE and Unsorted Index** are exclusively for Apply Join Index. For explicit-positional encoding (RLE or Index), the table’s left section applies when m_1 and m_2 are sorted, with only the upper triangular matrix shown due to symmetry. Note: Outputs from `rle_to_index` (Index) and `rle_to_plain` (Plain) serve as input for subsequent lookups in this table.

| | m_1 : RLE | m_1 : Plain | m_1 : Index | m_1 : Unsorted RLE | m_1 : Unsorted Index |
|---------------|--|--|---|--------------------------------------|---------------------------------|
| m_2 : RLE | $\left\{ \begin{array}{l} \text{range_intersect}(m_1, m_2) \\ \text{range_intersect}(m_2, m_1) \end{array} \right\}$ | $\left\{ \begin{array}{l} \text{rle_to_index}(m_2) \\ \text{rle_to_plain}(m_2) \end{array} \right\}$ | $\left\{ \begin{array}{l} \text{idx_in_rle}(m_1, m_2) \\ \text{rle_contain_idx}(m_1, m_2) \end{array} \right\}$ | $\text{range_intersect}(m_1, m_2)$ | $\text{idx_in_rle}(m_1, m_2)$ |
| m_2 : Plain | | $m_1 \& m_2$ | $m_1[m_2[m_1]]$ | $\text{rle_to_index}(m_1)$ | $m_1[m_2[m_1]]$ |
| m_2 : Index | | | $\left\{ \begin{array}{l} \text{idx_in_idx}(m_1, m_2) \\ \text{idx_in_idx}(m_2, m_1) \end{array} \right\}$ | $\text{rle_contain_idx}(m_2, m_1)$ | $\text{idx_in_idx}(m_1, m_2)$ |

Table 3: Output *MaskColumn* encoding for AND Operation. The table is symmetric and we only show the upper triangular matrix for better readability.

| | m_1 : RLE | m_1 : Plain | m_1 : Index |
|---------------|-------------|---------------|---------------|
| m_2 : RLE | RLE | Plain/Index | Index |
| m_2 : Plain | | Plain | Index |
| m_2 : Index | | | Index |

The output encoding for the AND operation appears in Table 3. Intuitively, the characteristics of the input layouts dictate the resulting output layout. For instance, if both inputs use RLE, their masks are typically continuous, so the output is also continuous and best encoded as RLE. However, if one input is RLE (ranges) and the other is Index (points), the resulting mask is likely discontinuous, making the Index representation more appropriate.

5.2 OR

We outline the design of this operator in Table 4, and show the encoding of the result in Table 5.

Table 4: Implementation design of Physical Operator for OR between *MaskColumns* m_1 and m_2 . Since OR is commutative, the table is symmetric and we only show the upper triangular matrix for better readability.

| | m_1 : RLE | m_1 : Plain | m_1 : Index |
|---------------|---------------------------------|--|---|
| m_2 : RLE | $\text{range_union}(m_1, m_2)$ | $\left\{ \begin{array}{l} \text{rle_to_index}(m_2) \\ \text{rle_to_plain}(m_2) \end{array} \right\}$ | $\left\{ \begin{array}{l} \text{idx_in_rle}(m_1, m_2) \\ \text{rle_contain_idx}(m_1, m_2) \end{array} \right\}$ |
| m_2 : Plain | | $m_1 \mid m_2$ | $m_2[m_1] = T$ |
| m_2 : Index | | | $\left\{ \begin{array}{l} \text{merge_sorted_idx}(m_1, m_2) \\ \text{merge_sorted_idx}(m_2, m_1) \\ \text{concat_sort}(m_1, m_2) \end{array} \right\}$ |

Table 5: Output *MaskColumn* encoding for OR Operation. The table is symmetric and we only show the upper triangular matrix for better readability.

| | m_1 : RLE | m_1 : Plain | m_1 : Index |
|---------------|-------------|---------------|---------------|
| m_2 : RLE | RLE | Plain | RLE + Index |
| m_2 : Plain | | Plain | Plain |
| m_2 : Index | | | Index |

- **Plain mask OR Plain mask:** This is a simple boolean OR operation using PyTorch’s logical OR operator (`()`). For example, if we have two Plain masks $[T, F, T, F]$ and $[T, T, F, F]$, the result would be $[T, T, T, F]$.
- **RLE mask OR RLE mask:** This operation computes the union of two sorted lists of ranges. We identify the start and end points of consecutive True values by computing differences. Non-overlapping segments are then determined using a mask.

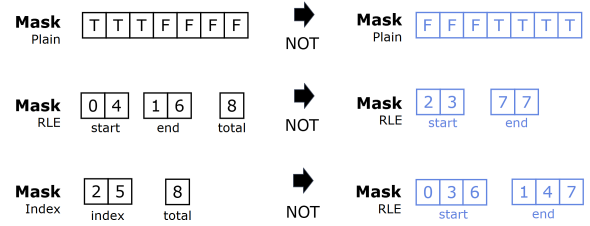


Figure 3: Illustration of NOT logical operator.

- **RLE mask OR Plain mask:** To perform this operation efficiently, we first convert the RLE mask into either an Index mask (`rle_to_index`) or a Plain mask (`rle_to_plain`), and then apply the OR operation. The choice depends on the sparsity of the RLE mask: if sparse, convert to an Index mask; otherwise, convert to a Plain mask.
- **RLE Mask OR Index Mask:** This involves bucketizing based on the relative sizes of the RLE and Index masks. We use either the Index mask to bucketize the RLE mask (`idx_in_rle`) or use the RLE mask to bucketize the Index mask (`rle_contain_idx`).
- **Plain Mask OR Index Mask:** This operation is performed using PyTorch’s subscript (`[]`) operator.
- **Index Mask OR Index Mask:** This operation merges two sorted Index tensors (`merge_sorted_idx`). For efficiency, we bucketize the larger tensor. A flag tracks the origin of each element, and the final merge is performed using a conditional selection (`‘where’`). If both Index tensors are small, the most efficient approach is to simply concatenate and sort them.

5.3 NOT

Finally, we describe the NOT logical operator, which takes a single *MaskColumn* as input and produces an output *MaskColumn*.

- **NOT Plain mask:** This is a straightforward bitwise negation using PyTorch’s complement (`~`) operator.
- **NOT RLE mask:** We use the `complement_rle` primitive. The key idea is to compute the gaps between consecutive runs. Each gap starts at the end of the previous run plus one and ends at the start of the next run minus one. This requires an additional metadata to track the total number of the rows in the column.
- **NOT Index mask:** We use the `complement_index` primitive. Similar to the RLE case, we compute gaps between indices, and need to keep track of the column size. Notably, the output is in RLE format rather than an Index representation. This is because Index *MaskColumns* are assumed to be sparse, making their NOT result more continuous and thus well-suited for RLE.

EXAMPLE 5. Consider applying the NOT operator to the three different mask representations shown in Figure 3:

- **NOT on Plain mask.** For a Plain mask $[T, T, T, F, F, F, F]$, we simply apply PyTorch’s bitwise negation operator (\sim) to flip each boolean value, resulting in $[F, F, F, T, T, T, T]$.
- **NOT on RLE mask.** For an RLE mask with $s = [0, 4]$, $e = [1, 6]$, and $total_size = 8$, we apply the `complement_rle` primitive. First, we compute the potential start points, s' , for inverted ranges by concatenating $[-1]$ with the original end values and adding 1. $s' = [0, 2, 7]$. Then, we compute potential end points, e' , by concatenating the original start values with $[total_size]$ and subtracting 1. $e' = [-1, 3, 7]$. We keep only the valid ranges where $s' \leq e'$, which gives us $s' = [2, 7]$ and $e' = [3, 7]$. This is an RLE mask covering the gaps between the original runs.
- **Step 3: NOT on Index mask.** For an Index mask with $p = [2, 5]$ and $total_size = 8$, we apply the `complement_index` primitive. We compute potential start points by concatenating $[-1]$ with the original indices and adding 1. $s = [0, 3, 6]$. We compute potential end points by concatenating the original indices with $[total_size]$ and subtracting 1. $e = [1, 4, 7]$. After applying a validity mask to ensure $s \leq e$, $s < total_size$, and $e \geq 0$, all position ranges remain valid. This is an RLE Mask with runs covering all positions not in the original Index mask.

5.4 Operating on Composite MaskColumns

To apply the previously described logical operators to Composite (Plain + Index, or RLE + Index) masks, we extend our approach accordingly. A key observation is that a Composite *MaskColumn* layout is essentially an OR operation between mask tensors. This allows us to leverage Boolean algebra (De Morgan’s Law, Associative and Distributive rules) to rewrite logical operations on Composite masks. Let $m(RLE)$ and $m(Index)$ represent the RLE and Index tensors of Composite mask m .

- **NOT:** $\neg(m_1(RLE) \vee m_1(Index)) = (\neg m_1(RLE)) \wedge (\neg m_1(Index))$
- **OR:** $(m_1(RLE) \vee m_1(Index)) \vee (m_2(RLE) \vee m_2(Index)) = (m_1(RLE) \vee m_2(RLE)) \vee (m_1(Index) \vee m_2(Index))$
- **AND:** $(m_1(RLE) \vee m_1(Index)) \wedge (m_2(RLE) \vee m_2(Index)) = (m_1(RLE) \wedge m_2(RLE)) \vee (m_1(RLE) \wedge m_2(Index)) \vee (m_1(Index) \wedge m_2(RLE)) \vee (m_1(Index) \wedge m_2(Index))$

Note that the sub-operations can all be performed in parallel using multiple CUDA streams. The encoding of the result *MaskColumn* is RLE for NOT operator, and Composite for OR and AND operators.

6 ARITHMETIC, COMPARISON, AND SELECTION OPERATIONS

Next, we focus on a general class of operators whose results are a point-wise/position-wise operation on values from two input columns, for positions that are common to both columns. This includes the logical AND operator that we discussed in Section 5.1, binary arithmetic operators, comparison operators, and selection operators using a filter predicate. Joins need additional handling that we discuss in Section 8. The logical OR operator that we discussed in Section 5.2 does not fit into this category in the general case since the result covers a union of the set of positions from the input columns which can be larger than the set of positions for any one

column in the presence of gaps (e.g., due to a prior filter operation being applied to the column, and the result not being compacted thereafter).

The main challenge in performing these operations on compressed inputs is that, in contrast to Plain encoding, there is no longer an alignment between positional representations of the inputs. Thus, point-wise operations are not directly possible. Instead, we need to first align the positional representations of the inputs, including the value tensors as needed, and then perform the operations on the aligned segments. We call this an *Alignment* operation.

EXAMPLE 6. Consider the operation $A+B$ on input columns A and B which are both in RLE format. $A.v = [4, 1, 3]$, $A.s = [0, 10, 20]$, $A.e = [9, 19, 39]$; $B.v = [6, 8]$, $B.s = [0, 15]$, $B.e = [14, 39]$. Thus, A has 3 runs of lengths 10, 10, and 20 and B has 2 runs of lengths 15 and 25. Similar examples apply for other operators such as $-$, $*$, $/$, $<$, $>$, $=$, etc.

Note that due to the misalignment of runs, we cannot directly do $A.v + B.v$. Although in this example the two columns have different runs, misalignment can happen even with the same number of runs but differences in run lengths for at least one run.

To perform this operation, we first align the runs of the input columns. This is exactly how we handle the AND operator (Section 5.1) with an additional step of reconstructing the value (v) tensors for the result. In this example, the result of the alignment operation would be two RLE columns R_1 and R_2 with $R_1.s = R_2.s = [0, 10, 15, 20]$, $R_1.e = R_2.e = [9, 14, 19, 39]$, $R_1.v = [4, 1, 1, 3]$, $R_2.v = [6, 6, 8, 8]$. Both columns have identical s and e tensors. We can now do a point-wise addition of the value tensors to get the value for the 4 runs in the result: $R_1.v + R_2.v = [10, 7, 9, 11]$.

The operation is simple if one of the operands is a scalar expression or literal, e.g., $A * 2$, $1 - A$, $A \geq 3$, etc. in which case we do not need to align anything but instead just operate on the value tensors for both RLE and Index encoding.

For selection operations with a filter predicate, e.g., *SELECT A FROM D WHERE P*, we first compute a *MaskColumn* m according to the evaluation of predicate P , then align m and A , and finally apply m to the tensor representations of A (if needed). Since m only tracks True values for RLE and Index encoding, the alignment step itself causes the selection and the final application step is not needed for those cases. However, if m or A is Plain encoded, then the final mask application step is needed to get the result.

7 GROUP-BY-AGGREGATION OPERATIONS

For aggregation queries, the process is decomposed into two phases.

- (1) **Grouping:** Partitioning rows according to the group-by columns.
- (2) **Aggregating:** Computing summary statistics (e.g., SUM, COUNT, AVG, MIN, MAX) for each identified group.

Both phases are conceptually straightforward in PyTorch—function `torch.unique` can handle grouping by building inverse indices based on the unique values in the group-by columns, and function `torch.scatter` can handle aggregation based on these inverse indices. However, the challenge lies in managing heterogeneous compression schemes across *DataColumns*. For example, consider a query that groups by two columns, one of which is RLE-compressed and the other is Plain. The `torch.unique` function will not work because it requires two Plain *DataColumns*, but the values of the

RLE column are not aligned with those of the Plain column. This heterogeneity prevents the direct application of `torch.unique` and `torch.scatter` due to misalignment in the data representations. To solve this problem, we apply our novel Alignment technique, described in Section 6, to both the Grouping and Aggregating phases.

7.1 Grouping Phase

The grouping phase constructs an inverse index that maps each row to its corresponding group; rows in the same group share the same data values across the group-by columns. It takes a set of aligned *DataColumns* for the group-by (potentially non-compact) as input and returns an inverse index. The inverse index is a single tensor from 0 to N-1, where N is the number of unique values across the group-by columns. The length of the inverse index is the same as the number of values in the group-by columns—for Plain data, it is the number of rows; for RLE and Index data, it is the number of RLE runs or index points.

7.2 Aggregating Phase

The aggregation operator takes a set of aligned *DataColumns* (for aggregation), the inverse index (from the grouping phase), and an aggregation function as input, and returns a set of tensors (one for each column to be aggregated) containing the aggregated results. The length of these tensors is the same as the number of unique values across the group-by columns.

To implement aggregation, we apply the `torch.scatter` function to the data columns, scattering based on the inverse indices. This approach efficiently computes aggregates like SUM, COUNT, AVG, STD, VAR, MIN, and MAX for each group. Note, however, that if the data is RLE-compressed, each value in the data column must be repeated based on its corresponding RLE range size. Therefore, we need to account for this when scattering the data. This depends on the aggregation function.

- **MIN, MAX:** These functions are unaffected by compression and we only need to consider the value tensor: $min(v)$, $max(v)$.
- **SUM, COUNT:** For RLE columns, instead of expanding the data and counting/summing individual values, we compute the run lengths: $l = e - s + 1$. This is sufficient for COUNT. For SUM, we multiply the run lengths by the values ($v * l$).
- **AVG, STD, VAR:** These functions can be computed as a post-processing step after SUM and COUNT. For example, to compute AVG, we divide SUM by COUNT. To compute STD and VAR, we first compute the sum of the squared values, then use SUM and COUNT to calculate STD and VAR.

EXAMPLE 7. Consider a SQL query "SELECT SUM(B) GROUP BY A" on RLE-compressed data as shown in Figure 4. The input consists of a group-by column A with values [A, B, A] spanning runs [0 – 1], [2 – 4], [5 – 8] and a sum column B with values [0, 3, 8] spanning the same runs [0 – 1], [2 – 4], [5 – 8].

- **Step 1: Grouping.** We apply the grouping operation on the group-by column to identify unique groups. Using `torch.unique` on the values [A, B, A], we identify two unique groups (A and B) and generate an inverse index, $x = [0, 1, 0]$ that maps each run to its corresponding group: the first run (group-by value A) maps to group 0, the second run (group-by value B) maps to group 1,

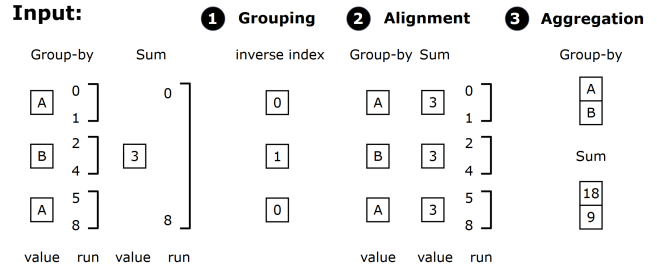


Figure 4: RLE-compressed data Group-by Aggregation: Grouping, Alignment and Aggregation steps illustrated.

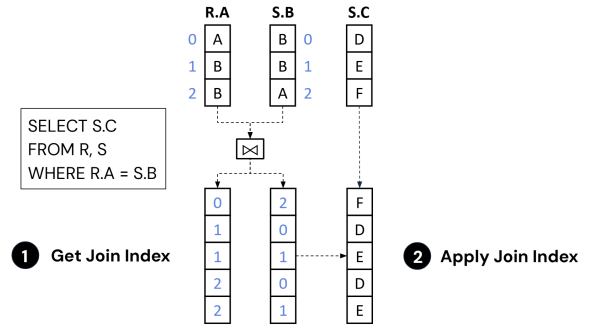


Figure 5: Illustration of join operation execution for the query "SELECT S.C FROM R, S WHERE R.A = S.B".

and the third run (group-by value A) again maps to group 0. This creates a temporary RLE column g with $v = x$ and with s and e the same as that of the group-by column (A).

- **Step 2: Alignment.** Next, we align g and the aggregation column (B). After alignment, as shown in the figure, both columns share the same runs [0 – 1], [2 – 4], and [5 – 8]. The aggregation column B is represented with aligned values [3, 3, 3] for these runs.
- **Step 3: Aggregation.** We do this in two steps—(a) perform a parallel aggregation for each segment in the aligned aggregation column by computing $v * l$ using its values [3, 3, 3] and run lengths [2, 3, 4], resulting in $[3 * 2, 3 * 3, 3 * 4] = [6, 9, 12]$, (b) perform a parallel aggregation for each group-by key by applying `torch.scatter` on the tensor [6, 9, 12] using the inverse index [0, 1, 0]. The scatter results in values $6 + 12 = 18$ (for group A, index 0) and 9 (for group B, index 1). We retrieve the group-by keys [A, B] corresponding to the inverse indices [0, 1].

8 JOIN OPERATIONS

We reuse TQP’s GPU-based hash join [18], used to join two Plain columns (from two tables) by building a hash table on one column (usually the smaller) and probing it with the other, but extend it to handle compressed columns (RLE and Index-encoded) as well. The join involves the following two steps.

- (1) **Get Join Index:** Two *Join Index* tensors are computed—one for each input column—that reference the rows in each column which match according to a join predicate. These *Join Index* tensors may be unsorted and contain duplicates (in case of one-to-many and many-to-many joins).
- (2) **Apply Join Index:** The *Join Index* tensors are applied to the columns participating in the join, to create the join result.

EXAMPLE 8. Consider the join operation illustrated in Figure 5 for the query “SELECT S.C FROM R, S WHERE R.A = S.B”. We have two tables: Table R with column A containing values [A, B, B] at positions 0, 1, and 2. Table S with column B containing values [B, B, A] and column C containing [D, E, F] at positions 0, 1, and 2.

The join operation executes as follows:

- **Step 1: Get Join Index.** We identify all pairs of positions where R.A equals S.B. R.A[0] = 'A' matches S.B[2] = 'A', creating the pair (0, 2). R.A[1] = 'B' matches both S.B[0] = 'B' and S.B[1] = 'B', creating pairs (1, 0) and (1, 1). Similarly, R.A[2] = 'B' also matches both S.B[0] and S.B[1], creating pairs (2, 0) and (2, 1). The resulting Join Index tensors are: Left index (for R): [0, 1, 1, 2, 2] (positions in R.A) and Right index (for S): [2, 0, 1, 0, 1] (positions in S.B).
- **Step 2: Apply Join Index.** We use the right index tensor to retrieve the corresponding values from S.C. This gives us S.C[2] = 'F' from the first match, S.C[0] = 'D' and S.C[1] = 'E' from the second and third matches (with R.A[1]), and S.C[0] = 'D' and S.C[1] = 'E' again from the fourth and fifth matches (with R.A[2]). The final result of the join is the column [F, D, E, D, E], which contains all values from S.C that correspond to matching rows between R.A and S.B. Note that because joins can create one-to-many relationships, the same value may appear multiple times in the result, and the output size may be larger than either input table.

In the remainder of this section, we discuss how we extend the two steps to join columns encoded for compression, *without first decompressing them*.

8.1 Get Join Index

Given two *DataColumns*, our goal is to implement a hash join on the two columns, such that the output is two *Join Index* tensors that reference the rows in each column which match according to a join predicate. Fortunately, the hashing and probing operations implementation for Plain columns can be reused directly for the value tensors of both RLE and Index *DataColumns*. The adaptations for each compressed layout are as follows.

- **RLE Data:** We perform a hash join on the RLE column’s value tensor, treating each run like a single row in the hash table. The resulting index references runs rather than individual rows. To map these run indices back to actual row indices, we re-expand by combining each run’s start/end range with the index tensor.
- **Index Data:** We hash join on the column’s value tensor, so the output indices initially reference the index entries themselves, not row positions. We then apply those indices to the original index tensor to recover the row positions for the final join.

The output of the hash join are two *Join Index* tensors, which are RLE or Index-encoded depending on the input *DataColumn* encodings. (Table 6).

Note that if either join column uses RLE, the matching index yields a one-to-many join and needs to be duplicated by the run length. If both join columns use RLE, then each pair of matching runs yields a many-to-many join, and the final run lengths are determined by the product of their lengths (by applying Algorithm 2 to duplicate the runs).

Table 6: *Join Index* encodings based on encodings of Input *DataColumns*. The *Join Index* tensors are unsorted and may contain duplicates. In each entry i, j of the table below, the top encoding is of the *Join Index* for the join column indicated by j and the bottom encoding is of the *Join Index* for the join column indicated by i .

| | RLE Data | Plain Data | Index Data |
|------------|--------------|----------------|----------------|
| RLE Data | RLE RLE | Index RLE | Index RLE |
| Plain Data | RLE Index | Index Index | Index Index |
| Index Data | RLE Index | Index Index | Index Index |

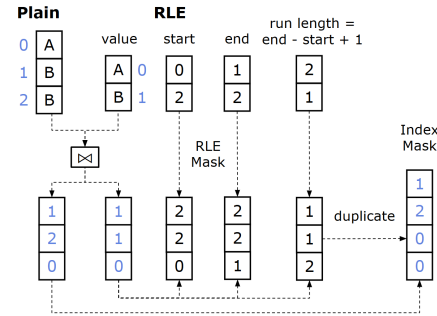


Figure 6: Illustration of computing *Join Indices* between Plain and RLE columns.

EXAMPLE 9. Consider generating *Join Indices* between a Plain *DataColumn* and an RLE *DataColumn* as shown in Figure 6. The Plain *DataColumn* contains values [A, B, B] at positions 0, 1, and 2. The RLE *DataColumn* contains values $v = [A, B]$ with start positions $s = [0, 2]$, end positions $e = [1, 2]$, and run lengths $l = [2, 1]$ ($l = e - s + 1$).

- **Step 1: Perform hash join on values.** We execute a hash join between the value arrays from both columns. This identifies that Plain[0] = 'A' matches RLE.value[0] = 'A', and Plain[1] = Plain[2] = 'B' matches RLE.value[1] = 'B'. The initial *Join Indices* are: [1, 2, 0] for the Plain column and [1, 1, 0] for the RLE column.
- **Step 2: Expand *Join Index* for Plain according to run lengths.** For each matched RLE run, we need to duplicate the corresponding Plain indices based on the run length. The RLE run with index 0 (value 'A') has a run length of 2, so the corresponding Plain index 0 is duplicated twice. The RLE run with index 1 (value 'B') has a run length of 1, so the corresponding Plain indices 1 and 2 are not duplicated.
- **Step 3: Generate final *Join Indices*.** The expanded *Join Index* for Plain becomes [1, 2, 0, 0] and the *Join Index* for RLE remains as RLE with $v = [1, 1, 0]$, $s = [2, 2, 0]$, $e = [2, 2, 1]$.

8.2 Apply Join Index

Once we have the *Join Indices*, we apply them to all participating *DataColumns* to generate the joined result. This is straightforward for the join columns. For other columns, we build on the same approach we developed earlier for filtering/selecting data (see Section 6), but extend it to handle unsorted or duplicate entries.

Table 2 outlines the extension needed for **Unsorted RLE** and **Unsorted Index MaskColumns**. For instance, suppose we want to

apply an RLE *Join Index* to an RLE *DataColumn*. Previously, if both sides were sorted, we used Algorithm 1 to bucketize whichever side was smaller for performance. This was valid because bucketize requires sorted input. Now, if one side is unsorted, we must bucketize the sorted side so that each run or index from the unsorted side can be matched to the corresponding runs in the sorted data.

This step can be further optimized for one-to-many and one-to-one joins, since there are no duplicates in the *Join Index* for the many-side of the join for the former case, and no duplicates in either *Join Index* for the latter case.

9 EXPERIMENTAL SETUP AND RESULTS

We compare our tensor-based GPU query execution on compressed data against tensor-based GPU query execution on Plain data (with dictionary encoding, like TQP)², and CPU-only query execution with SQL Server and Analysis Services [34]. We run GPU experiments on an Azure NC24ads A100 v4 VM [32] having an NVIDIA A100 GPU with 80 GiB HBM, 24 vCPUs, and 220 GiB main memory. For CPU-only analytics systems, we use an Azure D64s v5 VM [31] with 64 vCPUs and 256 GiB main memory. We report warm query times, averaged over multiple runs, after the data is loaded into memory (GPU HBM for GPU and main memory for CPU experiments) and caches have been warmed up. We monitor GPU memory usage with the `nvidia-smi` profiling tool.

We select input table column encodings using simple heuristics.

- Columns under 1M rows use Plain encoding.
- Else, if the RLE compression ratio > 20, then use RLE.
- Else, if many single-element runs exist but longer runs still yield an RLE compression ratio > 20, then use RLE+Index.
- Else, if removing top/bottom 5% of values allows a narrower type for the remaining data, then use Plain+Index.
- Else, use Plain encoding (possibly centered).

9.1 TPC-H Queries

We evaluate our approach using a subset of TPC-H queries (Q1, Q2, Q6, Q11, Q14, Q15, Q17, Q19) at scale factors (SF) 50, 100, and 300. The TPC-H benchmark utilizes synthetic data which, compared to real-world datasets (discussed in Section 9.2), exhibits limited sparsity and redundancy. This characteristic makes techniques like V-order [33] less effective for general compression across all queries. Therefore, to optimize for compression, we employ query-specific sort orders for the relevant tables based on the columns involved in each query’s filters and joins, as detailed in Table 7. Sorting significantly improves RLE effectiveness by increasing average run lengths and reducing the total number of runs. For instance, as illustrated for the `l_returnflag` column in Q1 at SF=50 (Figure 7), sorting reduces the number of runs from >105M to just 3, while increasing the average run length from 2.86 to slightly over 100M.

Figures 8 and 9 present the peak GPU memory usage and query run times, respectively, comparing query execution performance on uncompressed (Plain) data versus compressed (RLE, Index) data formats across SF 50, 100, and 300. Our evaluation reveals substantial benefits when processing compressed data directly on the GPU.

²Execution plans on Plain data are an optimized version of the tensor programs generated by TQP. Plain performance are therefore equal or better than TQP.

Peak memory usage (Figure 8) is significantly reduced; for example, at SF=300, Q19 requires 65.3 GiB with Plain data but only 17.5 GiB with compressed data (a 3.7× reduction). Compression enables processing larger scale factors like SF=300 for queries such as Q1 and Q17, which exceed the 80 GiB GPU memory limit with Plain data. Query run times (Figure 9) are also dramatically reduced, with speedups often exceeding 10×. For instance, at SF=300, Q6 runs 17.3× faster (68.6 ms vs 3.96 ms) and Q19 runs 23.8× faster (470.1 ms vs 19.8 ms) on compressed data. These results highlight the effectiveness of our techniques in improving both memory efficiency and performance for TPC-H queries on GPUs.

Using SQL Server query times for SF=50 as reference, the sum of times for the 8 queries running on GPU with compressed data was 12.8x lower for SF=50 and 2.6x lower for SF=300 (6x larger SF)!

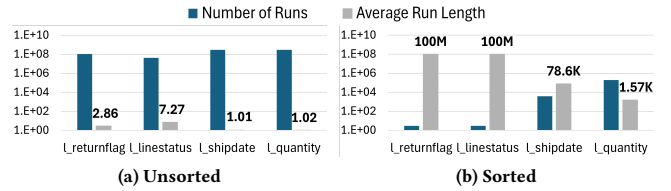


Figure 7: Total number of runs and average run lengths (with data labels) for RLE-compressed fact table columns for TPC-H SF=50 Q1 before and after sort.

Table 7: Query-specific column orderings for TPC-H.

| Query | Ordering Columns | Table |
|-------|--|----------|
| Q1 | l_returnflag, l_linestatus, l_shipdate, l_quantity | LINEITEM |
| Q2 | ps_suppkey, ps_partkey | PARTSUPP |
| | p_size, p_type, p_mfg, p_partkey | PART |
| Q6 | l_quantity, l_discount, l_shipdate | LINEITEM |
| Q11 | s_nationkey | SUPPLIER |
| | ps_suppkey | PARTSUPP |
| Q14 | l_shipdate | LINEITEM |
| | p_type | PART |
| Q15 | l_shipdate | LINEITEM |
| | l_partkey | LINEITEM |
| Q17 | p_brand, p_container, p_partkey | PART |
| | l_partkey | LINEITEM |
| Q19 | p_brand, p_container, p_size, p_partkey | PART |

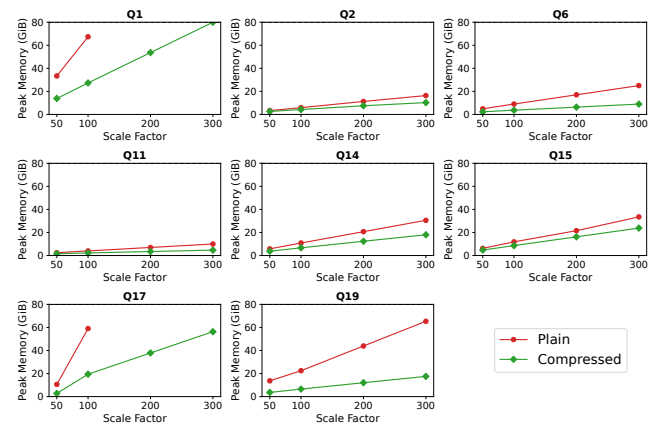


Figure 8: Peak GPU memory used while running TPC-H queries on Plain and Compressed input data for different SF.

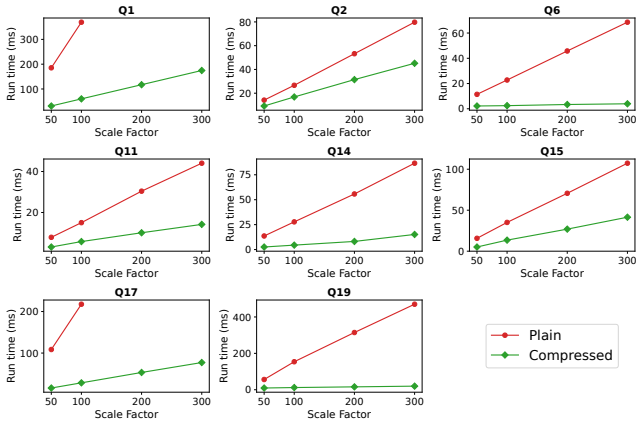


Figure 9: TPC-H query run times, using A100 GPU, on Plain and Compressed input data for different SF.

9.2 Production queries

We evaluate our methods using representative production queries on a first-party production dataset. It has a star schema with a large fact table having 2.94 Billion rows and 13 small dimension tables. It also has 4 ‘bridge’ tables that enable joins between the fact table and 4 of the dimension tables. On disk, each table is stored as V-ordered Parquet files [33], which is enabled by default in Microsoft Fabric. V-ordering applies sorting on tables, dictionary encoding, and other techniques to improve compression while supporting fast reads. Unlike in the TPC-H study (Section 9.1), we use the same input files, and thus the same row ordering for a given table, for all queries.

Table 8: Columns of the fact table used by the queries.

| Query | Columns of fact table used | Total used |
|-------|---|------------|
| Q1 | 1, 2, 3, 4, 5, 10, 11, 12, 13, 14 | 10 |
| Q2 | 2, 3, 5, 6, 7, 8, 9, 10, 11, 12, 13, 15 | 12 |
| Q3 | 2, 3, 5, 6, 7, 8, 9, 10, 11, 12, 13, 15 | 12 |

We use three queries for this study. Table 8 shows columns of the fact table that each query uses. Q1 uses 10 columns while Q2 and Q3 use 12 columns each. Together, the queries use 15 columns which is a subset of the total columns in the fact table. Relational operations in the queries include predicate filters on dimension tables, joins and semi-joins, and group-by aggregation (SUM). Q1 includes 7 semi-joins and 2 primary-key foreign-key (PK-FK) joins, Q2 and Q3 each includes 10 semi-joins and 1 PK-FK join. Q2 and Q3 have a similar template but differ in a filter predicate.

Figure 10 shows the sizes for the in-memory representation of the 15 columns of the fact table. The series ‘Plain’ refers to the default Plain encoding (with dictionary encoding) but with no other compression schemes applied. The total size for the 15 columns is 120.36 GiB with Plain and does not fit into the 80 GiB GPU HBM. Considering only the subset of columns needed by the specific queries, Q1 needs 87.53 GiB and Q2 and Q3 need 82.06 GiB, which is still larger than the GPU HBM capacity. The bottom row of the x-axis shows the encoding scheme for Compressed—‘C’: Composite (Plain + Index), ‘R’: RLE, ‘P’: Plain with bit-width reduction based on the range of values. The total size for 15 columns with Compressed is 56.84 GiB. For Q1 columns it is 43.69 GiB and for Q2 and Q3 it is 30.86 GiB, which can fit in the GPU HBM and also leave space for

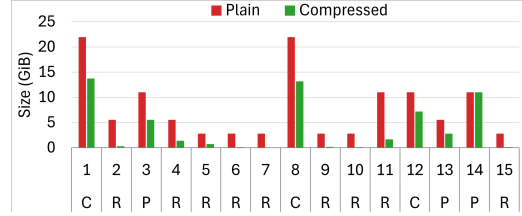


Figure 10: Input column sizes for the 15 columns in the fact table for Plain and Compressed representations. The bottom row in the x-axis labels shows the encoding for each column in compressed representation—R: RLE, C: Composite (Plain + Index), P: Plain with bit-width reduction.

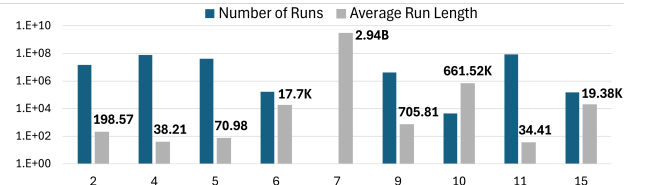


Figure 11: Total number of runs and average run lengths (with data labels) for RLE-compressed fact table columns.

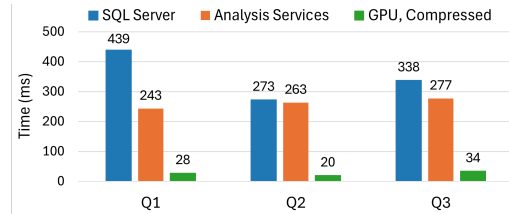


Figure 12: Query run times with Microsoft SQL Server on CPUs, Analysis Services on CPUs, and with our techniques for compressed input data on an A100 GPU.

intermediate results. For reference, the on-disk V-ordered file size for the projected fact table for the 15 columns is 29.87 GiB.

This production dataset has substantial opportunities for RLE compression. Figure 11 shows the number of runs and average run lengths in 7 of the 15 fact table columns that were compressed using RLE. Column 7 has a single run of 2.94B rows (same value for all rows). Average run lengths for other columns range from several tens to hundreds of thousands. For example, column 11 has 85.35M runs with an average run length of 34.41. Each run needs 20 bytes for representation—4 for value (v), 8 each for start (s) and end (e) positions. This requires 1.59 GiB memory for the column, which is significantly less than 10.94 GiB ($= 4 \times 2.94B$) needed for the Plain representation. Further savings are possible for RLE by using narrower data types for s and e .

Figure 12 shows query run times on state-of-the-art CPU-based commercial RDBMS, Microsoft SQL Server, and analytical data engine, Analysis Services. Our techniques lead to substantial speedups—15.75 (Q1), 13.66 (Q2), 9.82 (Q3), 12.76 (total) over SQL Server and 8.72 (Q1), 13.16 (Q2), 8.05 (Q3), 9.52 (total) over Analysis Services.

Finally, we study scalability characteristics by varying the input data size. For this we create smaller datasets with the first 5% (0.15B), 20% (0.6B), and 50% (1.5B) rows of the fact table. Figure 13 shows

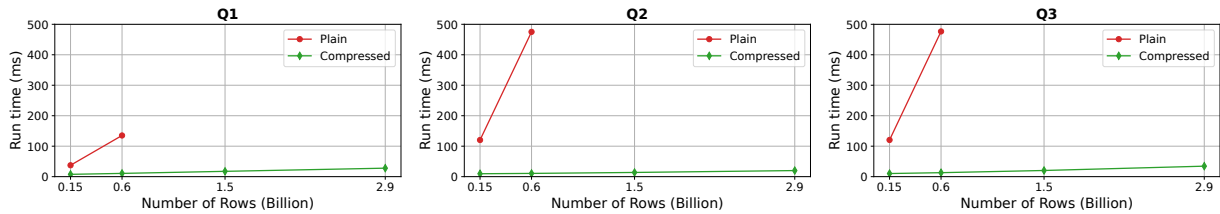


Figure 13: Run times for production queries, using A100 GPU, on Plain and Compressed data for different table sizes.

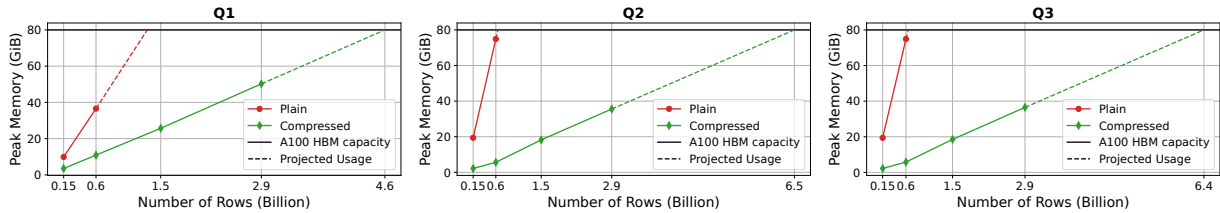


Figure 14: Peak GPU memory used and projected for production queries on Plain and Compressed data for different table sizes.

good performance scalability since GPU query times on compressed data increase much slower with data size compared to GPU query times on plain data. Queries cannot be run on Plain data for the 50% (and 100%) dataset due to running out of GPU HBM capacity, and Q2 and Q3 GPU times for just the 20% dataset exceed that of SQL Server and Analysis Services on CPUs for the 100% dataset! Thus, query execution on compressed data is necessary to unlock the GPU acceleration potential for this workload.

We could fit and process even larger datasets in the GPU HBM with our compression schemes. Figure 14 shows actuals and projections during query runs as we increase the fact table size. For Plain, we can only fit less than 50% of fact table rows whereas with Compressed we could go up to 157% (4.62B) for Q1, 222% (6.52B) for Q2, and 216% (6.36B) for Q3.

10 RELATED WORK

GPU acceleration for SQL analytics: There has been considerable research into using GPUs to accelerate SQL analytical queries [8–10, 13, 14, 18–21, 23, 28, 29, 35–39, 41, 45–49]. Rapid advances in GPU technology, to meet the needs of AI applications, continue to make GPUs increasingly attractive for SQL acceleration. Our work adds further support for this paradigm by developing new methods for GPU query processing on light-weight compressed data.

Query Execution over Compressed Data: The domain of query execution over compressed data has seen considerable research. Numerous studies have optimized dictionary encoding [12, 22, 26], among which C-store [3, 4] stands out as especially relevant. C-store introduces optimization strategies, such as rewriting summations as products over RLE and performing selections directly on the dictionary. Despite these advancements, two significant limitations exist: (1) Constricted design space: Previous works do not consider more complex scenarios where two RLE representations might select masks from each other, or where RLE representations are employed as group-by columns. Furthermore, we introduce a novel index representation, whose interaction with RLE has not previously been considered. The challenge in these studies is the amplified complexity associated with operator implementation [4, 51]. For our

case, this complexity is mitigated because we utilize PyTorch-based operators. Our work presents a comprehensive exploration of these scenarios. (2) CPU-centric designs: The majority of prior work focuses on CPU operations. In contrast, our designs and operators are fine-tuned specifically for GPUs, which fundamentally differ from CPUs. A GPU’s architecture emphasizes parallelism, necessitating each thread to manage simple tasks. This distinction raises a plethora of intriguing design questions.

Compression on GPU: Several works apply GPUs for query execution [7, 9, 11, 17, 18, 39] but are limited to only basic compression of dictionary encoding. With the challenges posed by limited GPU memory and PCIe bandwidth, many researchers have turned their attention to harnessing GPUs for compression [6, 15, 27, 36, 40, 42]. However, this compression typically facilitates only data transfer, and once the data is onboard the GPU, it often undergoes decompression, albeit potentially in a GPU-optimized manner. Existing works largely concentrate on refining the compression and decompression stages without addressing the direct end-to-end execution of queries in the encoded space.

RLE compression in data formats: RLE compression has wide support in both storage and in-memory data formats [1, 2, 5, 16, 24]. Reordering table rows to improve RLE compression has been leveraged in Microsoft Fabric [33], DuckDB [43], and others. We present new methods for SQL query processing to exploit the compression better for higher performance and smaller memory footprints.

11 CONCLUSION

We presented new methods for leveraging light-weight compression schemes to execute SQL analytics queries on GPUs directly on compressed data, with substantial reductions in GPU memory requirements and query run times. Our framework includes primitives for operating on encoded data, and implementations of relational operators including selection, group-by, aggregate, and join, that avoid decompression as far as possible. Our techniques result in significant acceleration of representative production queries on a real-world dataset compared to state-of-the-art commercial CPU analytics systems, and GPU query execution on uncompressed data.

REFERENCES

- [1] 2025 (last accessed). Arrow Columnar Format: Run-End Encoded Layout. [Online] Available from: <https://arrow.apache.org/docs/format/Columnar.html#run-end-encoded-layout>.
- [2] 2025 (last accessed). Vortex. [Online] Available from: <https://github.com/spiraldb/vortex>.
- [3] Daniel Abadi, Peter Boncz, and Stavros Harizopoulos. 2013. *The Design and Implementation of Modern Column-Oriented Database Systems*. Now Publishers Inc., Hanover, MA, USA.
- [4] Daniel Abadi, Samuel Madden, and Miguel Ferreira. 2006. Integrating Compression and Execution in Column-Oriented Database Systems. In *Proceedings of the 2006 ACM SIGMOD International Conference on Management of Data* (Chicago, IL, USA) (SIGMOD '06). Association for Computing Machinery, New York, NY, USA, 671–682. <https://doi.org/10.1145/1142473.1142548>
- [5] Azim Afrozeh and Peter Boncz. 2023. The FastLanes Compression Layout: Decoding > 100 Billion Integers per Second with Scalar Code. *PVLDB* 16, 9 (May 2023), 2132–2144. <https://doi.org/10.14778/3598581.3598587>
- [6] Azim Afrozeh, Lotte Felius, and Peter Boncz. 2024. Accelerating GPU Data Processing using FastLanes Compression. In *Proceedings of the 20th International Workshop on Data Management on New Hardware* (Santiago, AA, Chile) (DaMoN '24). Association for Computing Machinery, New York, NY, USA, Article 8, 11 pages. <https://doi.org/10.1145/3662010.3663450>
- [7] Yuki Asada, Victor Fu, Apurva Gandhi, Advitya Gemawat, Lihao Zhang, Dong He, Vivek Gupta, Ehi Nosakhare, Dalitso Banda, Rathijit Sen, and Matteo Interlandi. 2022. Share the tensor tea: how databases can leverage the machine learning ecosystem. *PVLDB* (2022), 3598–3601.
- [8] BlazingSQL. 2021. BlazingSQL. <https://github.com/BlazingDB/blazingsql>.
- [9] Jiashen Cao, Rathijit Sen, Matteo Interlandi, Joy Arulraj, and Hyesoon Kim. 2023. GPU Database Systems Characterization and Optimization. *PVLDB* 17, 3 (Nov. 2023), 441–454. <https://doi.org/10.14778/3632093.3632107>
- [10] Periklis Chrysogelos, Manos Karpathiotakis, Raja Appuswamy, and Anastasia Ailamaki. 2019. HetExchange: encapsulating heterogeneous CPU-GPU parallelism in JIT compiled engines. *Proc. VLDB Endow.* 12, 5 (Jan. 2019), 544–556. <https://doi.org/10.14778/3303753.3303760>
- [11] Wei Cui, Qianxi Zhang, Spyros Blanas, Jesús Camacho-Rodríguez, Brandon Haynes, Yinan Li, Ravi Ramamurthy, Peng Cheng, Rathijit Sen, and Matteo Interlandi. 2023. Query Processing on Gaming Consoles. In *Proceedings of the 19th International Workshop on Data Management on New Hardware* (Seattle, WA, USA) (DaMoN '23). Association for Computing Machinery, New York, NY, USA, 86–88. <https://doi.org/10.1145/3592980.3595313>
- [12] Patrick Damme, Annett Ungeth'um, Johannes Pietrzyk, Alexander Krause, Dirk Habich, and Wolfgang Lehner. 2020. Morphstore: Analytical query engine with a holistic compression-enabled processing model. *arXiv preprint arXiv:2004.09350* (2020).
- [13] Voltron Data. (last accessed) 2025. Theus The Enterprise SQL Engine. <https://voltrondata.com/>.
- [14] Yangshen Deng, Shiwon Chen, Zhaoyang Hong, and Bo Tang. 2024. How Does Software Prefetching Work on GPU Query Processing?. In *Proceedings of the 20th International Workshop on Data Management on New Hardware* (Santiago, AA, Chile) (DaMoN '24). Association for Computing Machinery, New York, NY, USA, Article 5, 9 pages. <https://doi.org/10.1145/3662010.3663445>
- [15] Wenbin Fang, Bingsheng He, and Qiong Luo. 2010. Database compression on graphics processors. *Proceedings of the VLDB Endowment* 3, 1-2 (2010), 670–680.
- [16] Apache Software Foundation. 2021. Apache Parquet. <https://parquet.apache.org/> Accessed: 2025-03-25.
- [17] Apurva Gandhi, Yuki Asada, Victor Fu, Advitya Gemawat, Lihao Zhang, Rathijit Sen, Carlo Curino, Jesús Camacho-Rodríguez, and Matteo Interlandi. 2022. The Tensor Data Platform: Towards an AI-centric Database System. In *CIDR*.
- [18] Dong He, Supun C Nakandala, Dalitso Banda, Rathijit Sen, Karla Saur, Kwanghyun Park, Carlo Curino, Jesús Camacho-Rodríguez, Konstantinos Karanasos, and Matteo Interlandi. 2022. Query Processing on Tensor Computation Runtimes. *PVLDB* (2022), 2811–2825.
- [19] HeavyDB. 2025 (last accessed). HeavyDB. <https://github.com/heavyai/heavydb>.
- [20] Kijae Hong, Kyoungmin Kim, Young-Koo Lee, Yang-Sae Moon, Sourav S Bhowmick, and Wook-Shin Han. 2025. Themis: A GPU-Accelerated Relational Query Execution Engine. *Proc. VLDB Endow.* 18, 2 (Feb. 2025), 426–438. <https://doi.org/10.14778/3705829.3705856>
- [21] Yu-Ching Hu, Yuliang Li, and Hung-Wei Tseng. 2022. TCUDB: Accelerating Database with Tensor Processors. In *Proceedings of the 2022 International Conference on Management of Data* (Philadelphia, PA, USA) (SIGMOD '22). Association for Computing Machinery, New York, NY, USA, 1360–1374. <https://doi.org/10.1145/3514221.3517869>
- [22] Hao Jiang, Chunwei Liu, John Papparrizos, Andrew A. Chien, Jihong Ma, and Aaron J. Elmore. 2021. Good to the Last Bit: Data-Driven Encoding with CodecDB. In *Proceedings of the 2021 International Conference on Management of Data* (Virtual Event, China) (SIGMOD '21). Association for Computing Machinery, New York, NY, USA, 843–856. <https://doi.org/10.1145/3448016.3457283>
- [23] Tomas Karnagel, René Müller, and Guy M. Lohman. 2015. Optimizing GPU-accelerated Group-By and Aggregation. In *ADMS@VLDB*. <https://api.semanticscholar.org/CorpusID:5017248>
- [24] Maximilian Kuschewski, David Sauerwein, Adnan Alhomssi, and Viktor Leis. 2023. BtrBlocks: Efficient Columnar Compression for Data Lakes. In *Proceedings of the 2023 ACM SIGMOD International Conference on Management of Data* (SIGMOD '23), 2205–2217.
- [25] Ryan M Layer, Kevin Skadron, Gabriel Robins, Ira M Hall, and Aaron R Quinlan. 2013. Binary Interval Search: a scalable algorithm for counting interval intersections. *Bioinformatics* 29, 1 (2013), 1–7.
- [26] Jae-Gil Lee, Guy Lohman, Konstantinos Morfonios, Keshava Murthy, Ippokratis Pandis, Lin Qiao, Vijayshankar Raman, Vincent Kalandai Samy, Richard Sidle, Knut Stolze, et al. 2014. Joins on encoded and partitioned data. *Proceedings of the VLDB Endowment* (2014).
- [27] Jing Li, Hung-Wei Tseng, Chunbin Lin, Yannis Papakonstantinou, and Steven Swanson. 2016. HippogriffDB: balancing I/O and GPU bandwidth in big data analytics. *PVLDB* 9, 14 (Oct. 2016), 1647–1658. <https://doi.org/10.14778/3007328.3007331>
- [28] Clemens Lutz, Sebastian Breß, Steffen Zeuch, Tilmann Rabl, and Volker Markl. 2020. Pump Up the Volume: Processing Large Data on GPUs with Fast Interconnects. In *Proceedings of the 2020 ACM SIGMOD International Conference on Management of Data* (Portland, OR, USA) (SIGMOD '20). Association for Computing Machinery, New York, NY, USA, 1633–1649. <https://doi.org/10.1145/3318464.3389705>
- [29] Tobias Maltenberger, Ivan Ilic, Ilin Tolovski, and Tilmann Rabl. 2022. Evaluating Multi-GPU Sorting with Modern Interconnects. In *Proceedings of the 2022 International Conference on Management of Data* (Philadelphia, PA, USA) (SIGMOD '22). Association for Computing Machinery, New York, NY, USA, 1795–1809. <https://doi.org/10.1145/3514221.3517842>
- [30] Wes McKinney. 2010. Data structures for statistical computing in python. In *Proceedings of the 9th Python in Science Conference*, Vol. 445, 51–56.
- [31] Microsoft. 2024. Dv5 sizes series. <https://learn.microsoft.com/en-us/azure/virtual-machines/sizes/general-purpose/dv5-series>
- [32] Microsoft. 2024. NC_A100_v4 sizes series. <https://learn.microsoft.com/en-us/azure/virtual-machines/sizes/gpu-accelerated/nc100v4-series>
- [33] Microsoft. 2024. Understand V-Order for Microsoft Fabric Warehouse. [Online] Available from: <https://learn.microsoft.com/en-us/fabric/data-warehouse/v-order>.
- [34] Microsoft. 2025. What is Analysis Services? [Online] Available from: <https://learn.microsoft.com/en-us/analysis-services/analysis-services-overview?view=asallproducts-allversions>.
- [35] Johns Paul, Shengliang Lu, and Bingsheng He. 2021. *Database Systems on GPUs*. Now Foundations and Trends.
- [36] Viktor Rosenfeld, Sebastian Breß, and Volker Markl. 2022. Query processing on heterogeneous CPU/GPU systems. *ACM Computing Surveys (CSUR)* 55, 1 (2022), 1–38.
- [37] Ran Rui, Hao Li, and Yi-Cheng Tu. 2020. Efficient Join Algorithms for Large Database Tables in a Multi-GPU Environment. *Proc. VLDB Endow.* 14, 4 (dec 2020), 708–720. <https://doi.org/10.14778/3436905.3436927>
- [38] Ran Rui and Yi-Cheng Tu. 2017. Fast Equi-Join Algorithms on GPUs: Design and Implementation. In *Proceedings of the 29th International Conference on Scientific and Statistical Database Management* (Chicago, IL, USA) (SSDBM '17). Association for Computing Machinery, New York, NY, USA, Article 17, 12 pages. <https://doi.org/10.1145/3085504.3085521>
- [39] Anil Shanbhag, Samuel Madden, and Xiangyao Yu. 2020. A Study of the Fundamental Performance Characteristics of GPUs and CPUs for Database Analytics. In *SIGMOD*, 1617–1632.
- [40] Anil Shanbhag, Bobbi W. Yogatama, Xiangyao Yu, and Samuel Madden. 2022. Tile-based Lightweight Integer Compression in GPU. In *Proceedings of the 2022 International Conference on Management of Data* (Philadelphia, PA, USA) (SIGMOD '22). Association for Computing Machinery, New York, NY, USA, 1390–1403. <https://doi.org/10.1145/3514221.3526132>
- [41] Panagiotis Sioulas, Periklis Chrysogelos, Manos Karpathiotakis, Raja Appuswamy, and Anastasia Ailamaki. 2019. Hardware-Conscious Hash-Joins on GPUs. In *2019 IEEE 35th International Conference on Data Engineering (ICDE)*, 698–709. <https://doi.org/10.1109/ICDE.2019.00068>
- [42] Evangelia Sitaridi. 2016. *GPU-acceleration of in-memory data analytics*. Columbia University.
- [43] Jim Stam. 2022. *Low overhead self-optimizing storage for compression in DuckDB*. Master's thesis. Universiteit van Amsterdam–Vrije Universiteit Amsterdam.
- [44] Oliphant Travis E. 2006. NumPy. <http://www.numpy.org/>.
- [45] Bowen Wu, Dimitrios Koutsoukos, and Gustavo Alonso. 2025. Efficiently Processing Joins and Grouped Aggregations on GPUs. *Proc. ACM Manag. Data* 3, 1, Article 39 (Feb. 2025), 27 pages. <https://doi.org/10.1145/3709689>
- [46] Bobbi Yogatama, Weiwei Gong, and Xiangyao Yu. 2025. Scaling your Hybrid CPU-GPU DBMS to Multiple GPUs. *Proc. VLDB Endow.* 17, 13 (Feb. 2025), 4709–4722. <https://doi.org/10.14778/3704965.3704977>

- [47] Bobbi W. Yogatama, Weiwei Gong, and Xiangyao Yu. 2022. Orchestrating data placement and query execution in heterogeneous CPU-GPU DBMS. *Proc. VLDB Endow.* 15, 11 (July 2022), 2491–2503. <https://doi.org/10.14778/3551793.3551809>
- [48] Yichao Yuan, Advait Iyer, Lin Ma, and Nishil Talati. 2025. Vortex: Overcoming Memory Capacity Limitations in GPU-Accelerated Large-Scale Data Analytics. arXiv:2502.09541 [cs.DB] <https://arxiv.org/abs/2502.09541>
- [49] Yuan Yuan, Rubao Lee, and Xiaodong Zhang. 2013. The Yin and Yang of Processing Data Warehousing Queries on GPU Devices. In *Proceedings of the VLDB Endowment (PVLDB)*, Vol. 6. 817–828.
- [50] Matei Zaharia, Reynold S. Xin, Patrick Wendell, Tathagata Das, Michael Armbrust, Ankur Dave, Xiangrui Meng, Josh Rosen, Shivaram Venkataraman, Michael J. Franklin, Ali Ghodsi, Joseph Gonzalez, Scott Shenker, and Ion Stoica. 2016. Apache Spark: a unified engine for big data processing. *Commun. ACM* 59, 11 (Oct. 2016), 56–65. <https://doi.org/10.1145/2934664>
- [51] Marcin Zukowski, Sandor Heman, Niels Nes, and Peter Boncz. 2006. Super-scalar RAM-CPU cache compression. In *22nd International Conference on Data Engineering (ICDE'06)*. IEEE, 59–59.